Supplementary Information

Thermal equilibria between conformers enable highly reliable single-fluorophore ratiometric thermometers

Tianruo Shen [a], *Xia Wu* [a], *Davin Tan* [a], *Zhaochao Xu* [b] and *Xiaogang Liu* [a,*]

[a] Fluorescence Research Group, Singapore University of Technology and Design, 8 Somapah Road, Singapore 487372, Singapore

[b] CAS Key Laboratory of Separation Science for Analytical Chemistry, Dalian Institute of Chemical Physics, Chinese Academy of Sciences, Dalian 116023, China

Contents

1. Experimental and computational methods

Materials

Table S1. Details of the chemicals for the experiments.

No.	Name	CAS No.	Company	Product No.
1	BD140	1201643-08-4	TCI	D4898
2	1,4-Dioxane (Diox)	123-91-1	TCI	D0860
3	Dimethyl Sulfoxide (DMSO)	67-68-5	TCI	D5293
4	Formamide (FM)	75-12-7	TCI	F0045
5	Ethanol (EtOH)	64-17-5	TCI	CT30
6	Acid Red 52	3520-42-1	TCI	A0600
7	LD688	51325-95-2	Exciton	06880
8	DCM	51325-91-8	Exciton	06490
9	Rhodamine 101	116450-56-7	Exciton	06399
10	Rhodamine 590	13161-28-9	Exciton	05903
11	Dimethylformamide (DMF)	68-12-2	VWR	23466.298
12	Ethylene Glycol (EG)	107-21-1	VWR	24041.297
13	Methylcyclohexane (MCH)	108-87-2	Honeywell	M37889
14	Rhodamine B	81-88-9	Sigma Aldrich	83689
15	Acetonitrile (ACN)	75-05-8	Sigma Aldrich	271004

Spectral measurements

The UV-vis absorption and emission spectra were recorded using Duetta Fluorescence and Absorbance Spectrometer from HORIBA Scientific. Temperatures were adjusted by use of EXT-400 Liquid Cooling System from Koolance Inc and TC1 Temperature Controller from Quantum Northwest Inc.

The UV-vis absorption and emission spectra for **BD140** were measured at 2.5 μM and 0.25 μM dye concentrations in MCH, Diox, DMF, DMSO, and FM, respectively. The UV-vis absorption and emission spectra for **LD688** were measured at 5 μM and 2.5 μM dye concentrations in Diox, EtOH, ACN, and DMSO, respectively. The UV-vis

absorption and emission spectra for **DCM** were measured at 5 μM and 1.5 μM dye concentrations in Diox, EtOH, ACN, and DMSO, respectively.

Quantum yield measurements

The quantum yields were calculated based on the relative measurement method.[1] We chose Rhodamine 101 as the reference dye for **BD140**, Rhodamine B, and Acid Red 52. Rhodamine 590 was selected as the reference dye for **LD688** and **DCM**.

Computational methods

All density functional theory (DFT)[2] and time-dependent density functional theory (TD-DFT)[3] calculations were performed using *Gaussian 16* program.[4] The molecular structures both in the ground state (S_0) and the first excited state (S_1) were optimized using M06-2X[5] functional and def2-SVP[6] basis set. Solvation effects in different solvents were considered using the SMD[7] solvent model for all calculations, with the state-specific (SS)[8, 9] formalism for correcting the excitation/de-excitation energies. All the optimized structures were confirmed at the local minima on the potential energy surfaces through the frequency calculations in both the ground state and first excited singlet state. The molecular structures were visualized by VMD software.[10]

2. Temperature-dependent spectra of Rhodamine B and Acid Red 52

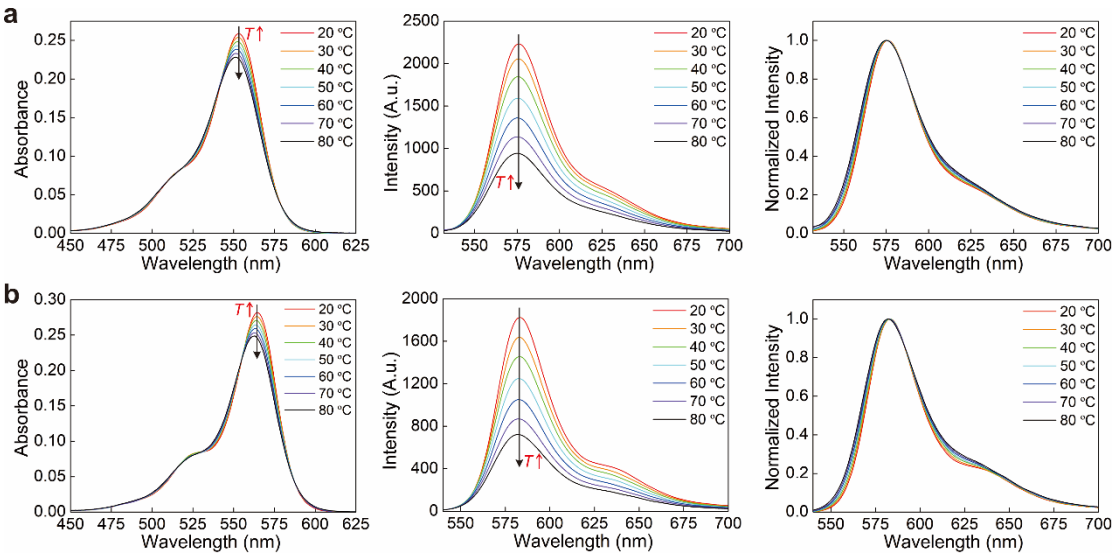

Figure S1. The UV-vis absorption (left), emission (middle), and normalized emission (right) spectra of (a) Rhodamine B and (b) Acid Red 52 in EG. Both of the two emission spectra were excited at 532 nm.

3. Optical properties and computational analysis of BD140

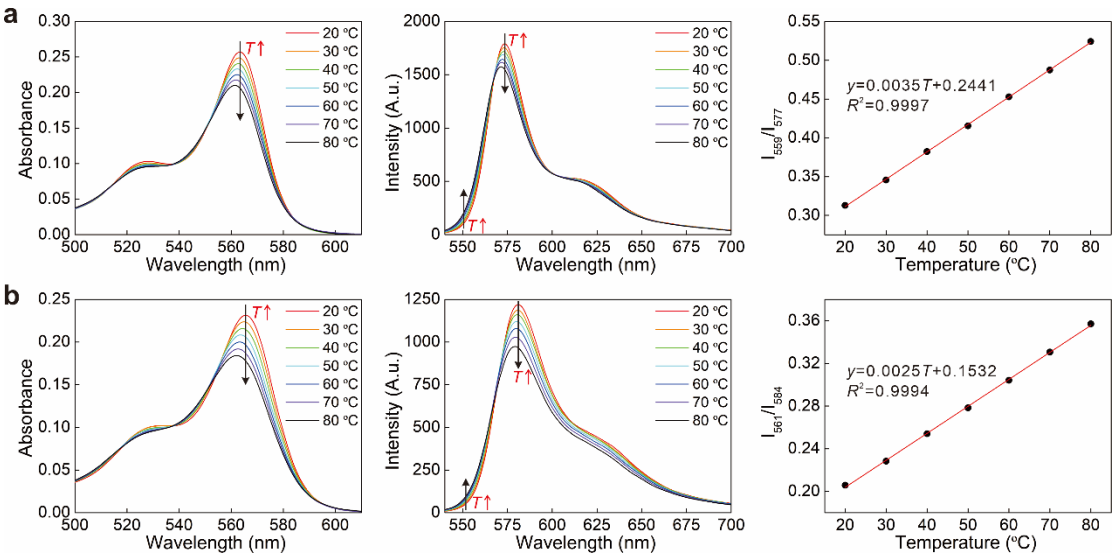

Figure S2. The UV-vis absorption (left), emission (middle) spectra and temperature-dependence of fluorescence intensity ratios with corresponding best linear fits (right) of **BD140** in (a) Diox (the ratio of fluorescence intensities at 559 nm and 577 nm) and (b) DMSO (the ratio of fluorescence intensities at 561 nm and 584 nm). Both of the two emission spectra were excited at 532 nm.

Table S2. Quantum yields of **BD140** in different solvents at various temperatures.

T (°C)	Quantum Yield				
	MCH	Diox	DMF	DMSO	FM
20	0.716	~1	0.956	0.955	0.876
30	0.714	~1	0.963	0.942	0.871
40	0.725	~1	0.956	0.952	0.845
50	0.727	~1	0.946	0.939	0.817
60	0.738	~1	0.912	0.928	0.795
70	0.719	~1	0.819	0.900	0.743
80	0.734	~1	0.863	0.866	0.680

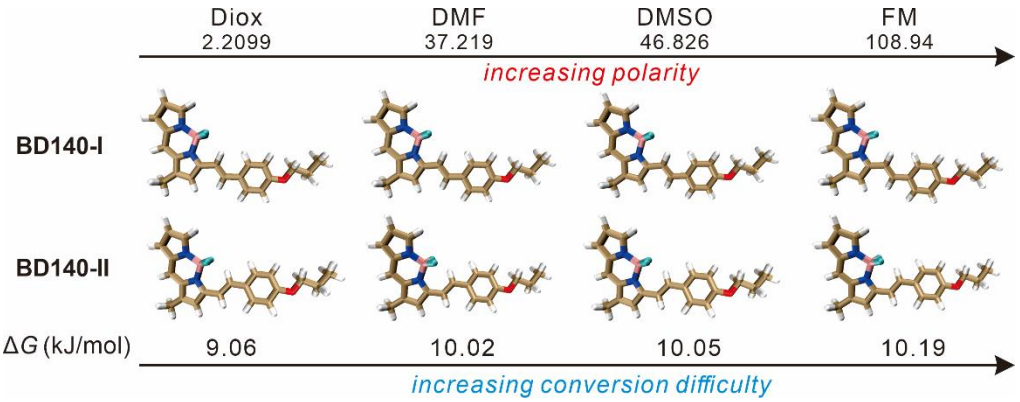

Figure S3. The optimized molecular structures of **BD140-I** and **BD140-II** with their relative Gibbs free energy ($\Delta G = G_2 - G_1$) at the ground state in Diox, DMF, DMSO, and FM.

4. Optical properties and computational analysis of LD688 and DCM

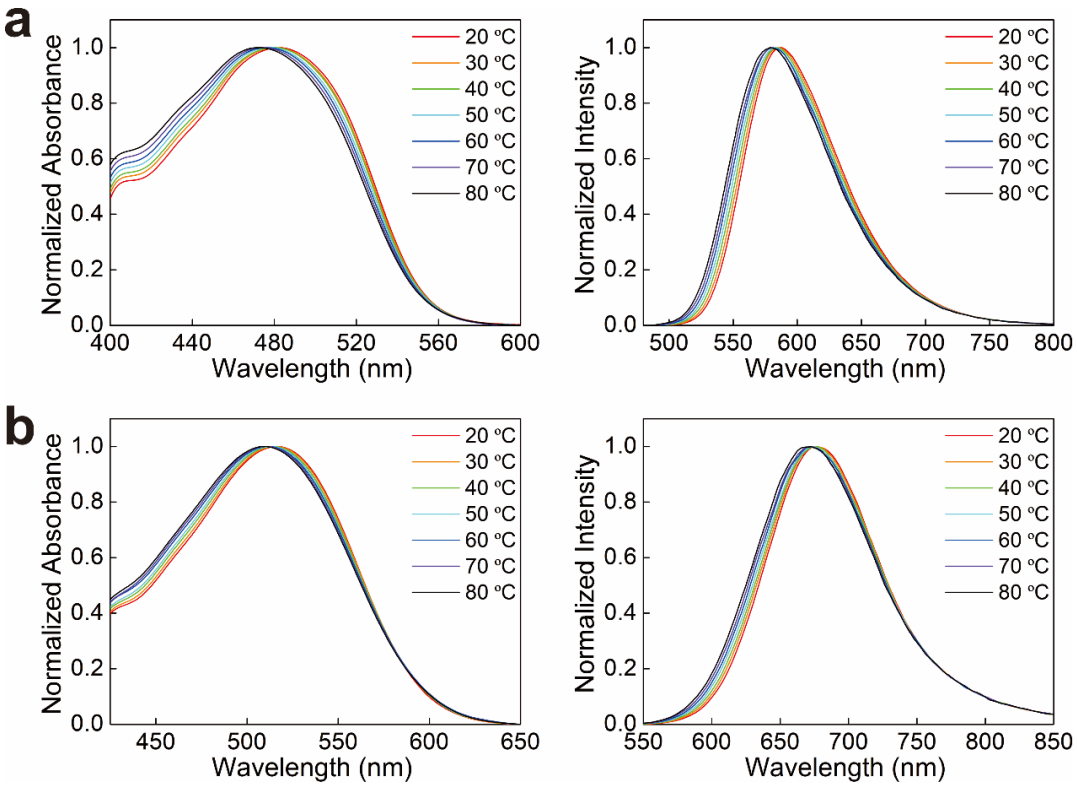

Figure S4. The normalized UV-vis absorption (left) and emission (right) spectra of **LD688** in (a) Diox and (b) DMSO.

Table S3. Quantum yields of **LD688** in Diox and DMSO at different temperatures.

Solvent	Quantum Yield						
	20 ℃	30 ℃	40 ℃	50 ℃	60 ℃	70 ℃	80 ℃
Diox	0.350	0.272	0.211	0.155	0.113	0.085	0.064
DMSO	0.173	0.149	0.126	0.108	0.093	0.080	0.070

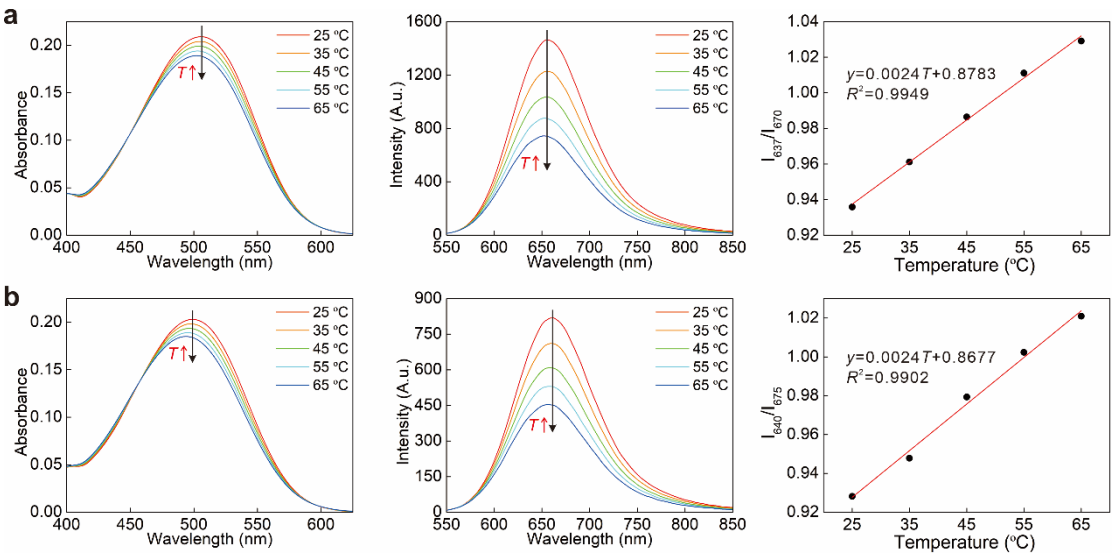

Figure S5. The UV-vis absorption (left), emission (middle) spectra and temperature-dependence of fluorescence intensity ratios with corresponding linear fitting equations (right) of **LD688** in (a) EtOH (the ratio of fluorescence intensities at 637 nm and 670 nm); (b) ACN (the ratio of fluorescence intensities at 640 nm and 675 nm). The emission spectra were excited at 505 nm and 495 nm, respectively.

Table S4. Quantum yields of **LD688** in EtOH and ACN at different temperatures.

Solvent	Quantum Yield				
	25 °C	35 °C	45 °C	55 °C	65 °C
EtOH	0.161	0.140	0.122	0.107	0.094
ACN	0.092	0.082	0.073	0.066	0.058

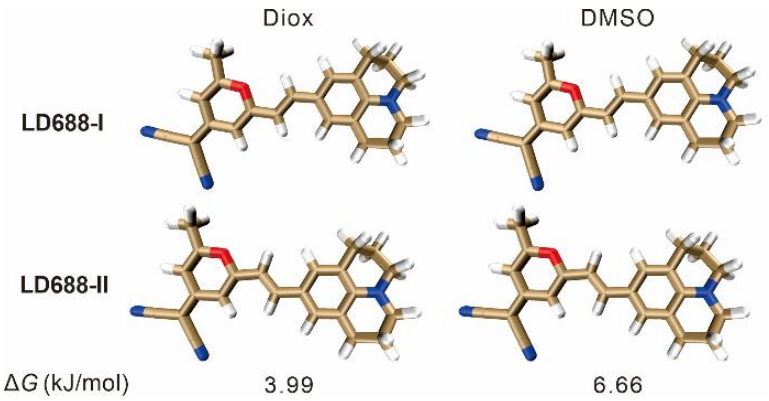

Figure S6. The optimized molecular structures of **LD688-I** and **LD688-II** and their relative Gibbs free energy ($\Delta G = G_2 - G_1$) at the ground state in Diox and DMSO.

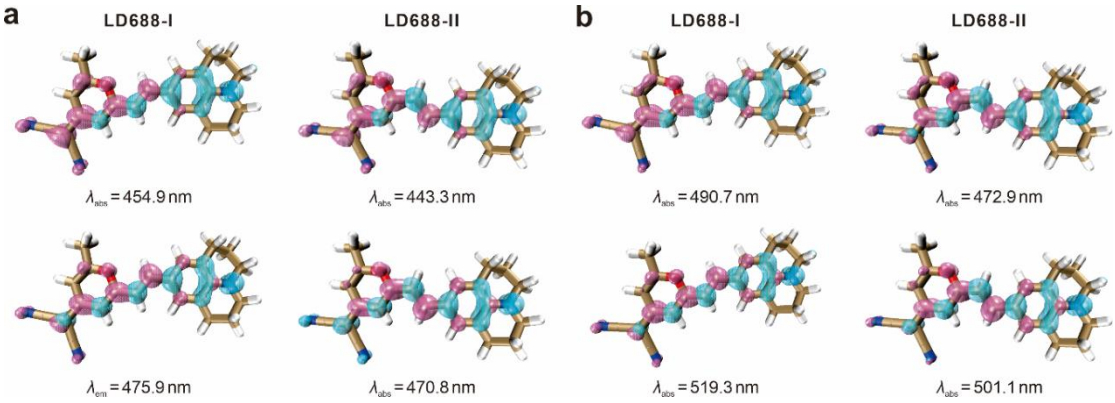

Figure S7. Optimized molecular structures with hole-electron distributions (cyan: hole, mauve: electron) of **LD688-I** and **LD688-II** at the ground state (top) and the first excited state (bottom) in (a) Diox and (b) DMSO. The insets show the calculated peak UV-vis absorption and emission wavelengths. Computational results show that the photoexcitation/photo-deexcitation to/from S_1 is dominated by the π-π* transitions between the highest occupied molecular orbital (HOMO) and the lowest unoccupied molecular orbital (LUMO) in **LD688**.

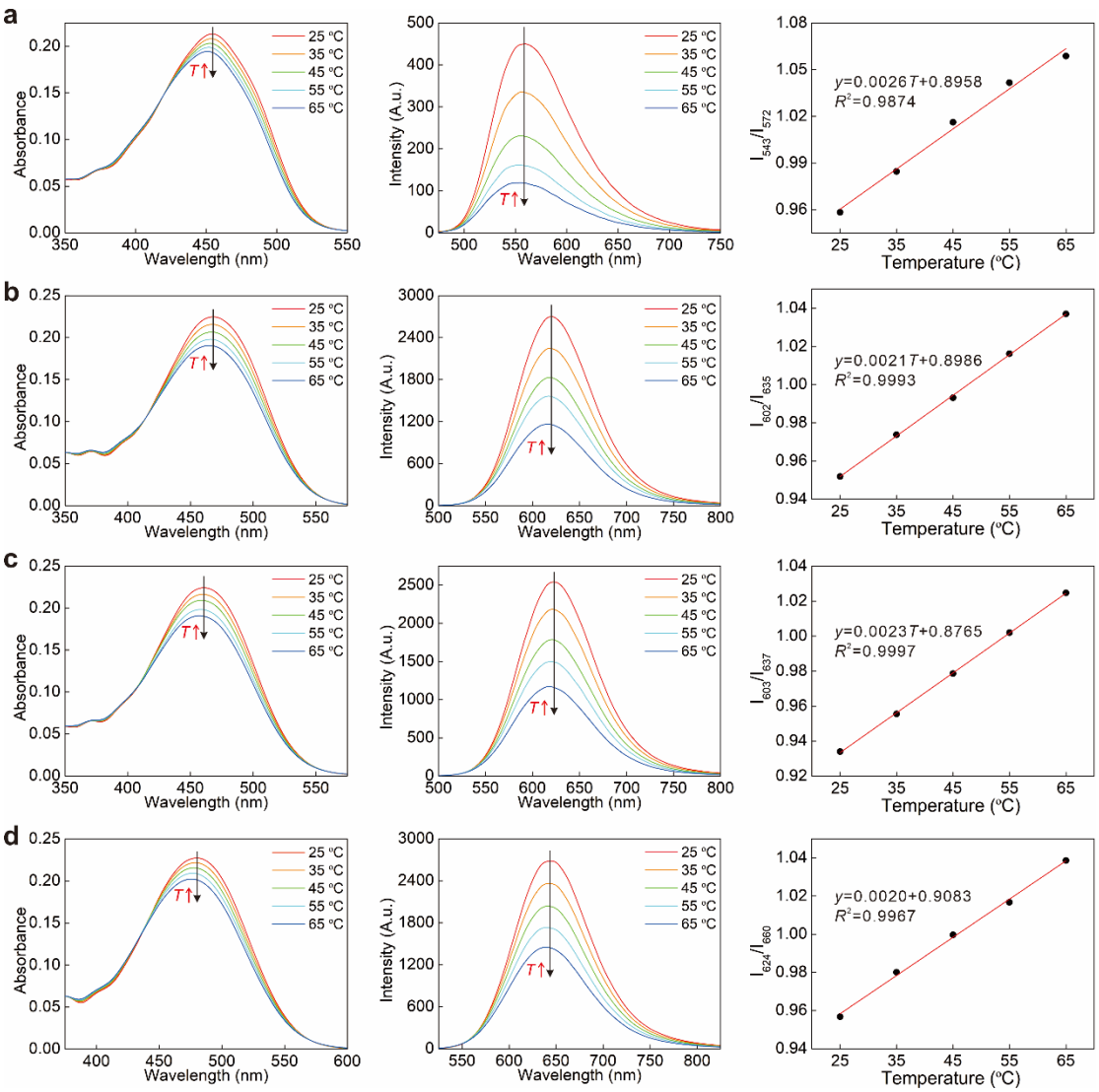

Figure S8. The UV-vis absorption (left), emission (middle) spectra and temperature-dependence of fluorescence intensity ratios with corresponding linear fitting equations (right) of **DCM** in (a) Diox (the emission spectrum were excited at 455 nm; the ratio of fluorescence intensities at 543 nm and 572 nm); (b) EtOH (the emission spectrum were excited at 470 nm; the ratio of fluorescence intensities at 602 nm and 635 nm); (c) ACN (the emission spectrum were excited at 460 nm, the ratio of fluorescence intensities at 603 nm and 637 nm); and (d) DMSO (the emission spectrum were excited at 480 nm; the ratio of fluorescence intensities at 624 nm and 660 nm).

Table S5. The quantum yields of **DCM** in four solvents at different temperatures.

Solvent	Quantum Yield				
	25 ℃	35 ℃	45 ℃	55 ℃	65 ℃
Diox	0.065	0.030	0.021	0.016	0.011
EtOH	0.391	0.343	0.295	0.265	0.208
ACN	0.344	0.309	0.264	0.236	0.194
DMSO	0.500	0.456	0.410	0.363	0.318

5. Reliability analysis of BD140 at different dye concentrations

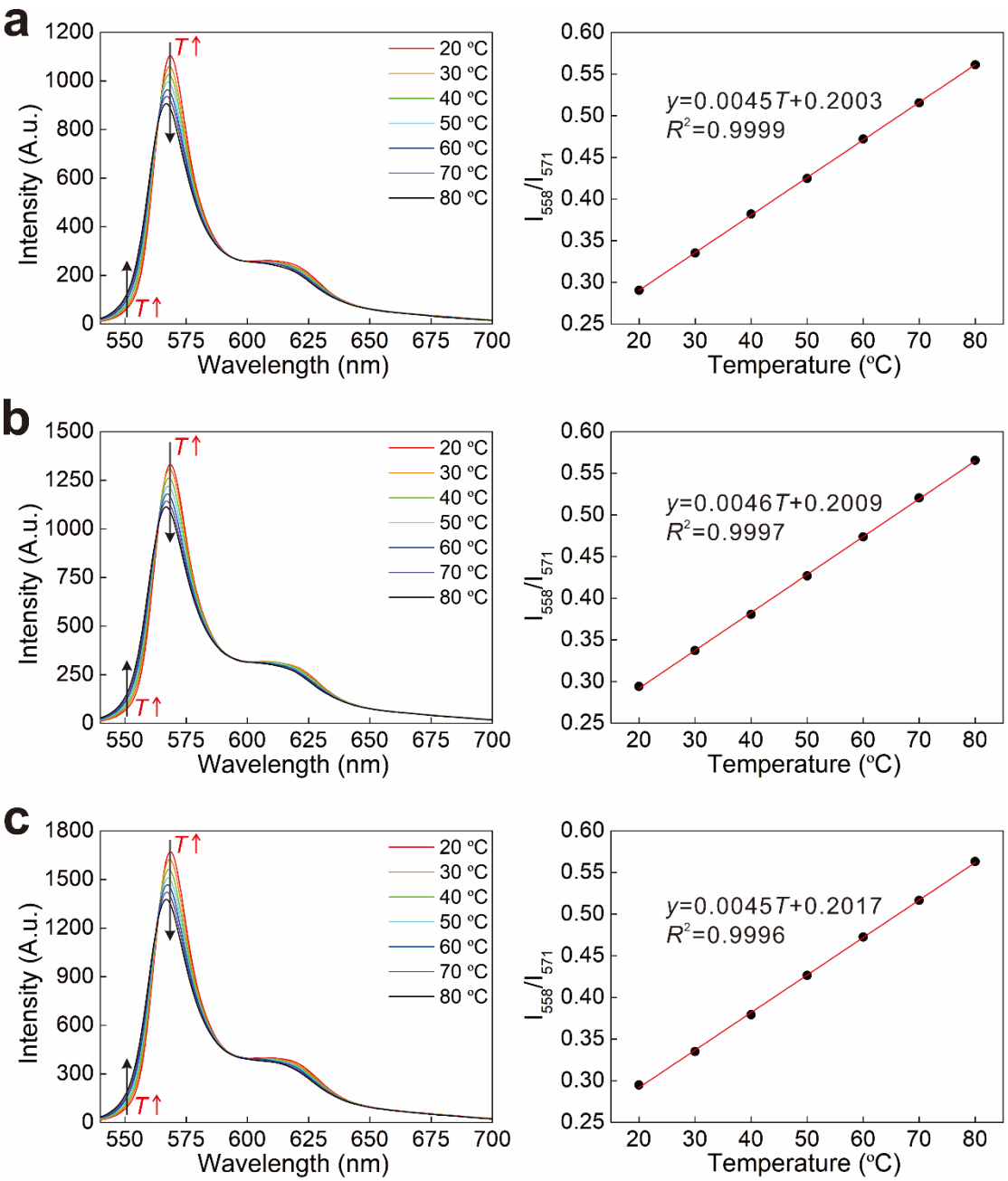

Figure S9. The emission spectra (left) and temperature-dependence of fluorescence intensity ratios with corresponding linear fitting equations (right) of **BD140** at (a) 0.200 μM, (b) 0.225 μM and (c) 0.275 μM in MCH. All the emission spectra were excited at 532 nm.

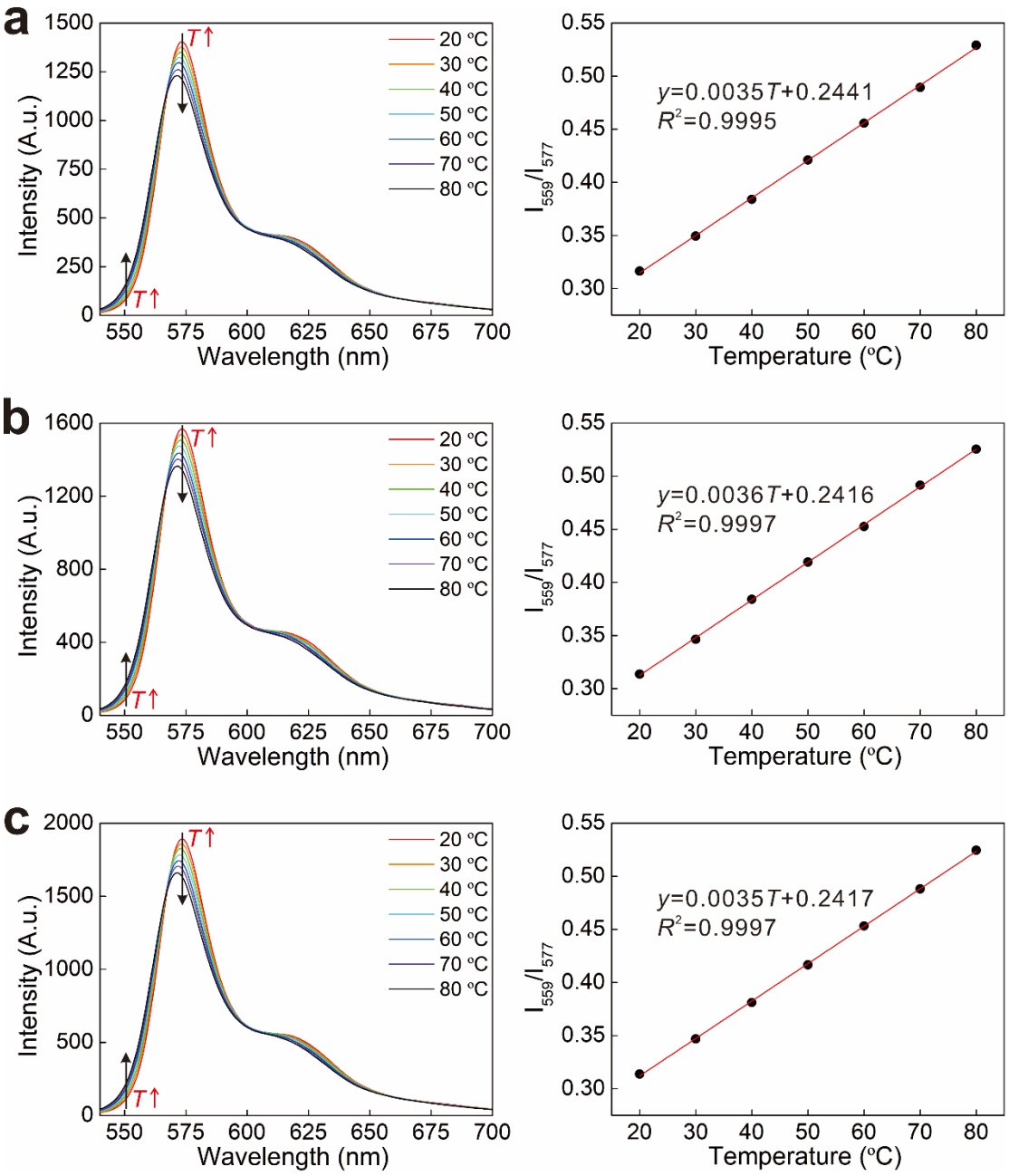

Figure S10. The emission spectra (left) and temperature-dependence of fluorescence intensity ratios with corresponding linear fitting equations (right) of **BD140** at (a) 0.200 μM, (b) 0.225 μM and (c) 0.275 μM in Diox. All the emission spectra were excited at 532 nm.

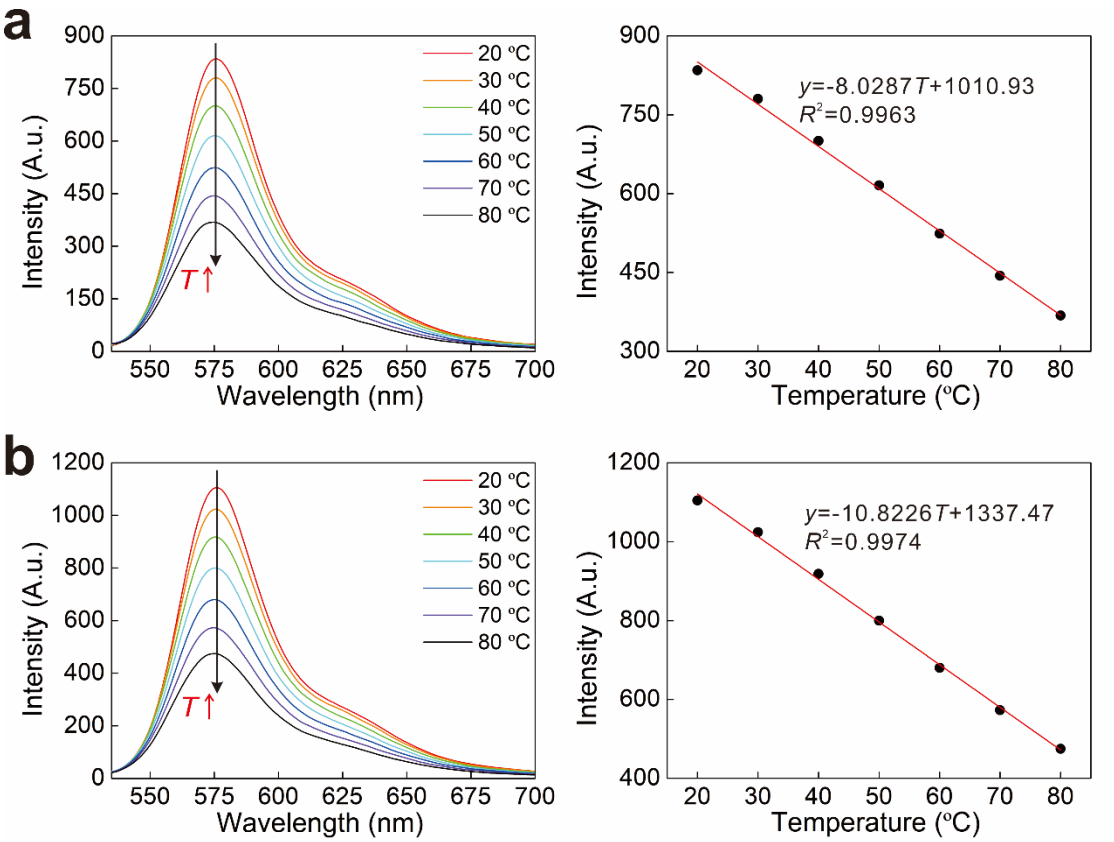

Figure S11. The emission spectra (left) temperature-dependence of fluorescence intensities at λ_{em} with corresponding linear fitting equations (right) for Rhodamine B at (a) 0.200 μM and (b) 0.250 μM.

6. References

1. C. Wurth, M. Grabolle, J. Pauli, M. Spieles and U. Resch-Genger, *Nat. Protoc.*, 2013, **8**, 1535-1550.
2. A. D. Becke, *J. Chem. Phys.*, 1993, **98**, 5648-5652.
3. G. Scalmani, M. J. Frisch, B. Mennucci, J. Tomasi, R. Cammi and V. Barone, *J. Chem. Phys.*, 2006, **124**, 94107.
4. M. J. Frisch, G. W. Trucks, H. B. Schlegel, G. E. Scuseria, M. A. Robb, J. R. Cheeseman, G. Scalmani, V. Barone, G. A. Petersson, H. Nakatsuji, X. Li, M. Caricato, A. V. Marenich, J. Bloino, B. G. Janesko, R. Gomperts, B. Mennucci, H. P. Hratchian, J. V. Ortiz, A. F. Izmaylov, J. L. Sonnenberg, D. Williams-Young, F. Ding, F. Lipparini, F. Egidi, J. Goings, B. Peng, A. Petrone, T. Henderson, D. Ranasinghe, V. G. Zakrzewski, J. Gao, N. Rega, G. Zheng, W. Liang, M. Hada, M. Ehara, K. Toyota, R. Fukuda, J. Hasegawa, M. Ishida, T. Nakajima, Y. Honda, O. Kitao, H. Nakai, T. Vreven, K. Throssell, J. A. Montgomery, Jr., J. E. Peralta, F. Ogliaro, M. J. Bearpark, J. J. Heyd, E. N. Brothers, K. N. Kudin, V. N. Staroverov, T. A. Keith, R. Kobayashi, J. Normand, K. Raghavachari, A. P. Rendell, J. C. Burant, S. S. Iyengar, J. Tomasi, M. Cossi, J. M. Millam, M. Klene, C. Adamo, R. Cammi, J. W. Ochterski, R. L. Martin, K. Morokuma, O. Farkas, J. B. Foresman, and D. J. Fox, Gaussian, Inc., Wallingford CT, 2016.
5. Y. Zhao and D. G. Truhlar, *Theor. Chem. Acc.*, 2007, **120**, 215-241.
6. F. Weigend and R. Ahlrichs, *Phys. Chem. Chem. Phys.*, 2005, **7**, 3297-3305.
7. A. V. Marenich, C. J. Cramer and D. G. Truhlar, *J. Phys. Chem. B*, 2009, **113**, 6378-6396.
8. R. Improta, V. Barone, G. Scalmani and M. J. Frisch, *J. Chem. Phys.*, 2006, **125**, 054103.
9. R. Improta, G. Scalmani, M. J. Frisch and V. Barone, *J. Chem. Phys.*, 2007, **127**, 074504.
10. W. Humphrey, A. Dalke and K. Schulten, *J. Mol. Graph.*, 1996, **14**, 33-38.